



Direct observation of grain boundaries in chemical vapor deposited graphene



Jong-Young Lee ^a, Ji-Hwan Lee ^a, Min Jung Kim ^a, Jatis Kumar Dash ^a, Chul-Ho Lee ^b, Rakesh Joshi ^c, Sunwoo Lee ^d, James Hone ^e, Aloysius Soon ^a, Gwan-Hyoung Lee ^{a,*}

^a Department of Materials Science and Engineering, Yonsei University, Seoul, 03722, South Korea

^b KU-KIST Graduate School of Converging Science and Technology, Korea University, Seoul, 02841, South Korea

^c Centre for Sustainable Materials Research and Technology (SMART), School of Materials Science and Engineering, University of New South Wales, Sydney, 2052, Australia

^d Department of Electrical and Computer Engineering, Cornell University, Ithaca, NY, 14853, USA

^e Department of Mechanical Engineering, Columbia University, New York, NY, 10027, USA

ARTICLE INFO

Article history:

Received 19 October 2016

Received in revised form

20 December 2016

Accepted 5 January 2017

Available online 9 January 2017

ABSTRACT

Graphene has received great attention owing to its superior physical properties, making graphene suitable for multiple applications. Numerous graphene growth techniques have been developed in the past decade to provide scalable high quality graphene. Among these techniques, chemical vapor deposition (CVD) on catalytic metal films holds great promises for a large-scale graphene growth. Even though extensive efforts have been devoted to synthesize high quality graphene, formation of defects. In particular, grain boundaries (GBs) have a dominant effect on properties, motivating extensive efforts to tune the CVD growth process to minimize GB. Rapid imaging of GBs will significantly aid in studies of CVD graphene grain structure. Here we report a straightforward technique to optically observe GBs in CVD-grown graphene *via* optical microscopy, allowing rapid assessment of graphene quality as well as the number of layers. The local oxidation of copper through the damaged GBs induces an optically discernable color change in the underlying copper due to different extend of oxidation between the two copper regions under grains and GBs. Our observation technique for GBs of graphene paves a path for understanding fundamental mechanisms of graphene growth and efficient quality evaluation of large-scale graphene sheet for mass production.

© 2017 Elsevier Ltd. All rights reserved.

1. Introduction

Graphene, a two dimensional one-atom-thick carbon nanomaterial, has received great attention owing to its superior physical properties, such as high carrier mobility, mechanical strength, flexibility, and transparency, which make graphene suitable for multiple applications [1–4]. Numerous graphene growth techniques have been developed in the past decade to provide scalable high quality graphene. Among these techniques, chemical vapor deposition (CVD) on catalytic metal films holds great promises for a large-scale graphene growth [5,6]. Even though extensive efforts have been devoted to synthesize high quality graphene [7–11], formation of defects, such as grain boundaries (GBs), impurities, vacancies, and ripples, is unavoidable during the growth and subsequent transfer processes, leading to the degradation of graphene

[3,11–14]. In particular, GBs have a dominant effect on properties [3,11–15], motivating extensive efforts to tune the CVD growth process to minimize GB *i.e.* to increase the grain size of graphene [8,9,16,17]. Despite significant improvements, more work is needed to fully understand and control grain structure in CVD-grown graphene. Rapid imaging of GBs will significantly aid in studies of CVD graphene grain structure. Typically, to probe microstructure of GBs, transmission electron microscopy (TEM) and scanning tunneling microscopy (STM) have been commonly used [18,19]. As an alternative, observation techniques, such as liquid crystal deposition, friction measurement, and UV-oxidation, have been proposed to examine the sizes and the shapes of graphene grains (domains) [20–23]. However, the aforementioned techniques suffer from complicated sample preparation processes and restricted observation areas. Therefore, a novel method for identification and examination of GBs of a large-scale graphene sheet is highly desired. Here we report a straightforward technique to optically

* Corresponding author.

E-mail address: gwanlee@yonsei.ac.kr (G.-H. Lee).

observe GBs in CVD-grown graphene *via* optical microscopy, allowing rapid assessment of graphene quality as well as the number of layers. Selective oxidation of underlying copper through graphene GBs with oxygen plasma followed by heating in air allows us to observe GBs *via* an optical microscope. GBs, which are line defects with structural instability and high energy, are damaged by oxygen plasma much faster than GB-free regions. The defective carbon lattices along the GBs accelerate thermal oxidation of underlying copper substrate. Our calculation of thermodynamic energy for GBs shows that oxygen can preferentially react with carbon at GBs due to the higher energy state of GBs. The local oxidation of copper through the damaged GBs induces an optically discernable color change in the underlying copper due to different extent of oxidation between the two copper regions under grains and GBs. Our observation technique for GBs of graphene paves a path for understanding fundamental mechanisms of graphene growth and efficient quality evaluation of large-scale graphene sheet for mass production.

2. Experimental

2.1. Sample preparation

The graphene was synthesized on a 25- μm -thick copper foil

(Alfa-Aesar, 99.8%) using low pressure chemical vapor deposition system (SciEnTech, TCVD50). After loading of the copper foil into the chamber, the temperature was rapidly elevated to 1000 °C for 10min. The copper foil was annealed for 1 h with a gas flow of H_2 (10 sccm) and graphene was synthesized by flowing H_2 (10 sccm) and CH_4 (25 sccm) for different time of 5–20 min. After completion of growth, the chamber was cooled down to room temperature, maintaining the gas flow rate of H_2 and CH_4 .

After synthesis, we transferred graphene on target substrate to further characterization. As-grown graphene on a copper foil was spin-coated with poly-methyl methacrylate (PMMA) at 3000 rpm for 1 min. The graphene grown on the bottom side of copper foil was removed by oxygen plasma. The copper foil was etched by ammonium persulfate (20 wt% solution) for 2 h, then PMMA/Graphene film is rinsed with DI water. PMMA/Graphene film was transferred to the SiO_2 substrate. Finally, the PMMA layer was dissolved in acetone.

2.2. Characterizations

The grain boundary observation through oxygen plasma and thermal oxidation is performed by conventional plasma generator and hot plate. The graphene grown on a copper foil was placed in a plasma chamber (Femto Science, Covance-1MPQ). To selectively

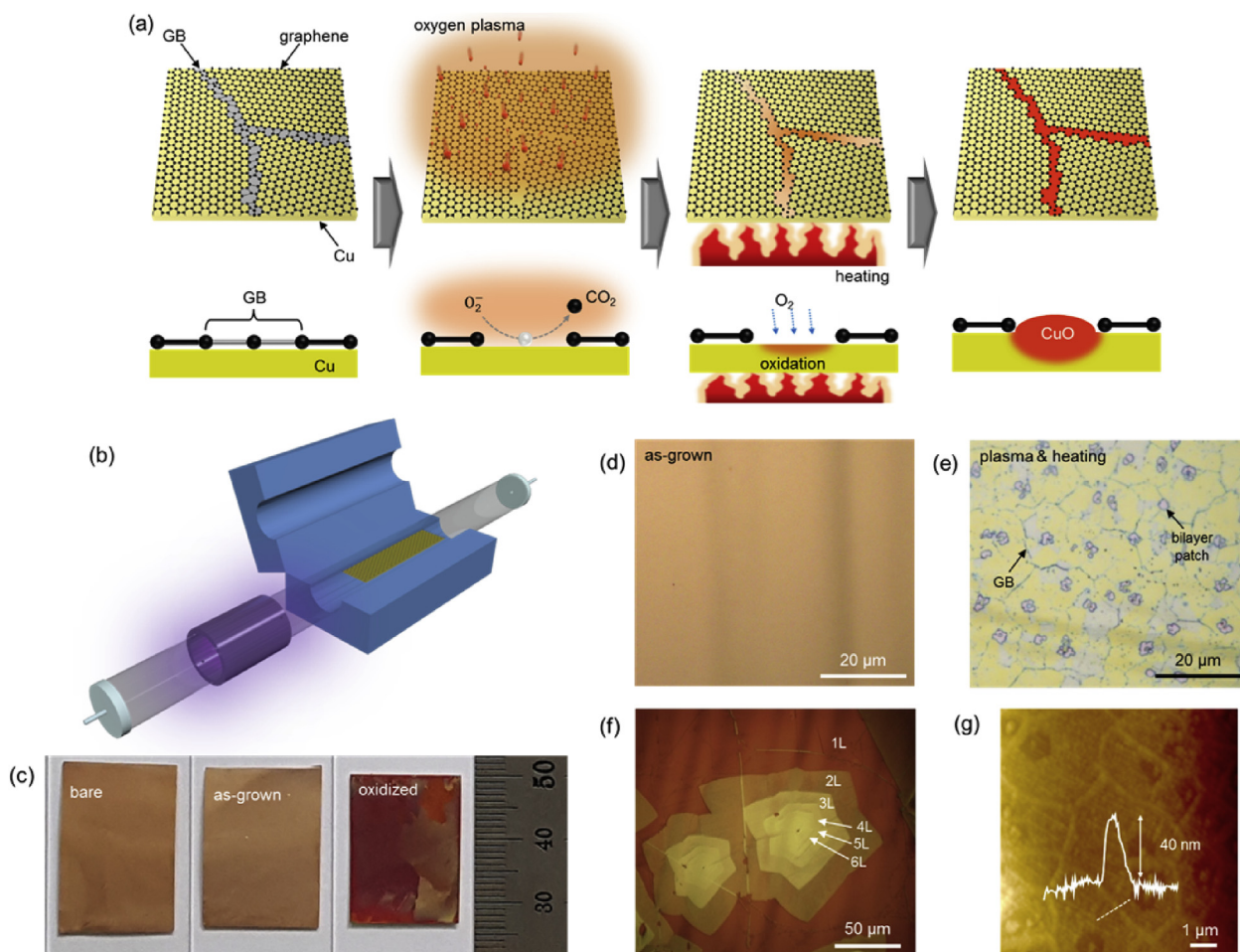


Fig. 1. (a) Schematics of GB observation technique *via* PATO process. (b) Schematic of CVD growth system incorporated with a plasma generator. (c) Optical images of copper foils: before graphene growth (bare), after graphene growth (as-grown), and after PATO process (oxidized). Optical micrographs of copper foils (d) after graphene growth (as-grown) and (e) after PATO process. (f) Optical micrograph of multilayer single crystal graphene on copper foil after PATO process. Number of layers is distinguishable due to distinct color contrast. (g) AFM image of CVD graphene on copper foil after PATO process. The line profile measured along the dashed line shows volume expansion of copper oxide at GB.

damage GBs of CVD graphene, oxygen plasma was generated in a gas flow of O_2 (20 sccm) with a power of 50 W and a fixed frequency of 50 kHz. Those parameters were varied changed (for power, 20–100 W; for time, 5–30 s). The plasma-treated CVD graphene was heated on a hot plate for thermal oxidation.

Raman measurements were conducted in the Raman spectroscopy (Renishaw, inVia) by using a diode-pumped solid state laser with 532 nm-wavelength and a spot size of 1 μm . We used 2 mW of power and 10 s for single measurement, and 0.5 s for mapping. SEM (Tescan, VEGA 3) and AFM (Park systems, NX10) were used to observe surface morphology of graphene grown on a copper substrate.

2.3. DFT calculation

For the density-functional theory (DFT) calculations, we have used the Vienna *ab initio* simulation package (VASP) code with the projector augmented wave (PAW) method to describe the ion-electron interactions [24,25]. The Kohn-Sham orbitals are

expanded with a plane-wave basis set and the kinetic cutoff energy is taken as 500 eV. The approximation to the DFT exchange-correlation (xc) functional is due to the recent work of Klimeš and co-workers (optB88-vdW) [26] where a self-consistent non-local van der Waals correction is applied. The detail of calculations is represented in the Supporting Information.

3. Results and discussion

The observation process of graphene GBs is schematically depicted in Fig. 1a. First, graphene was grown on a copper foil by CVD (See experimental section for CVD process). The grown graphene consists of small grains of a few micrometers, which are patched together through GBs [3,18]. The graphene grown on copper is treated with a weak oxygen plasma to selectively damage GBs, followed by heating the sample on a hot plate. During the heating, copper is partially oxidized through the damaged GBs. Thus we term this technique the plasma-assisted thermal oxidation (PATO) process. The oxidized region of the copper has a

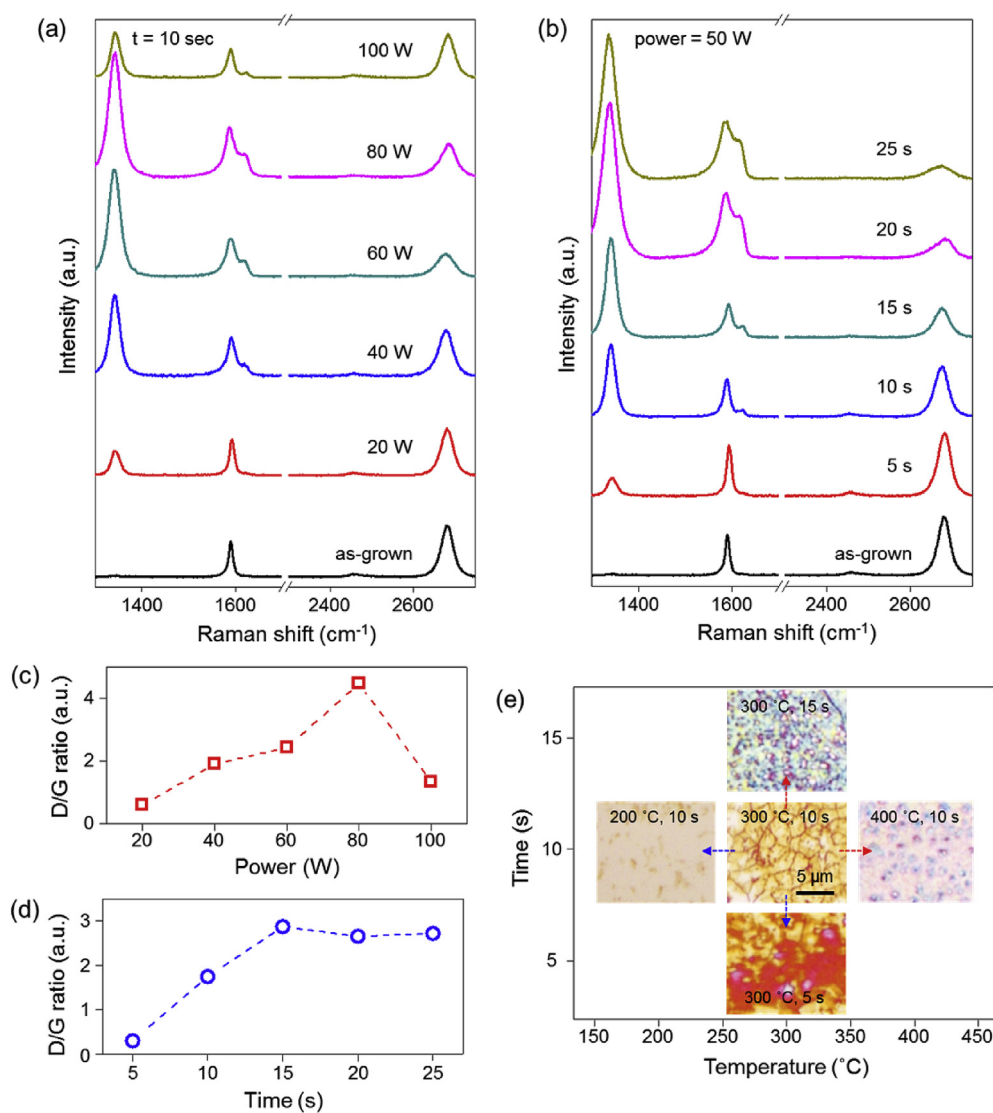


Fig. 2. Raman spectra of the CVD graphene samples treated (a) with various plasma generation powers for a fixed time of 10 s and (b) with a fixed plasma generation power of 50 W for various times. The D/G ratios of the CVD graphene samples treated (c) with various plasma generation power for a fixed time of 10 s and (d) with a fixed plasma generation power of 50 W for various times. (e) Optical micrographs of the CVD graphene samples on copper foils oxidized at different temperature and for different time. The GBs of graphene are most obviously observed when the sample was heated at 300 $^{\circ}\text{C}$ for 10 s.

distinguishable color so that the GBs can be directly observed through an optical microscope. The PATO process was systemized in a conventional CVD growth system by incorporating a plasma generator as shown in Fig. 1b. Fig. 1c shows optical images of copper foils: before growth (bare), after growth (as-grown), and after oxidation (oxidized). The bare copper and as-grown sample showed no difference in color, while oxidized copper exhibited orange color due to the formation of copper oxide. Fig. 1d shows an optical micrograph of the as-grown graphene film on copper, in which GBs are not visible. After the as-grown graphene was treated by oxygen plasma for 10 s and then heated at 300 °C for 10s, selective copper oxidation was accelerated through GBs as shown in the optical micrograph of Fig. 1e. The GBs of the graphene were clearly visible, enabling us to observe morphologies of grains and measure the grain size of the graphene. The grain size of the synthesized graphene (5–10 μm) and the stitched shape of grains are similar to previous reports [3,18]. As indicated by the arrow in

Fig. 1e, brighter bilayer patches of CVD graphene can be distinguished from monolayer region thanks to the different oxidation rates of copper under monolayer and bilayer graphene. Similarly, the graphene grown by ‘Pita-method’ [7], which has large graphene single crystals with multilayers, showed well-defined optical contrast due to the layer-thickness-dependent oxidation rate (Fig. 1f). It should be noted that the combination of plasma treatment and thermal heating is more effective for observing grain boundaries and multilayer patches, compared to individual application of oxygen plasma treatment and thermal heating (Figs. S1 and S2). After the PATO process, the thickness at GBs was increased by ~40 nm as shown in the AFM image of Fig. 1g, consistent with the formation of copper oxide along GBs.

The oxidation process was optimized to generate defects of adequate density and preferentially damage GBs with high selectivity. For the plasma treatment condition, we chose the plasma generation power and time as variables because these two

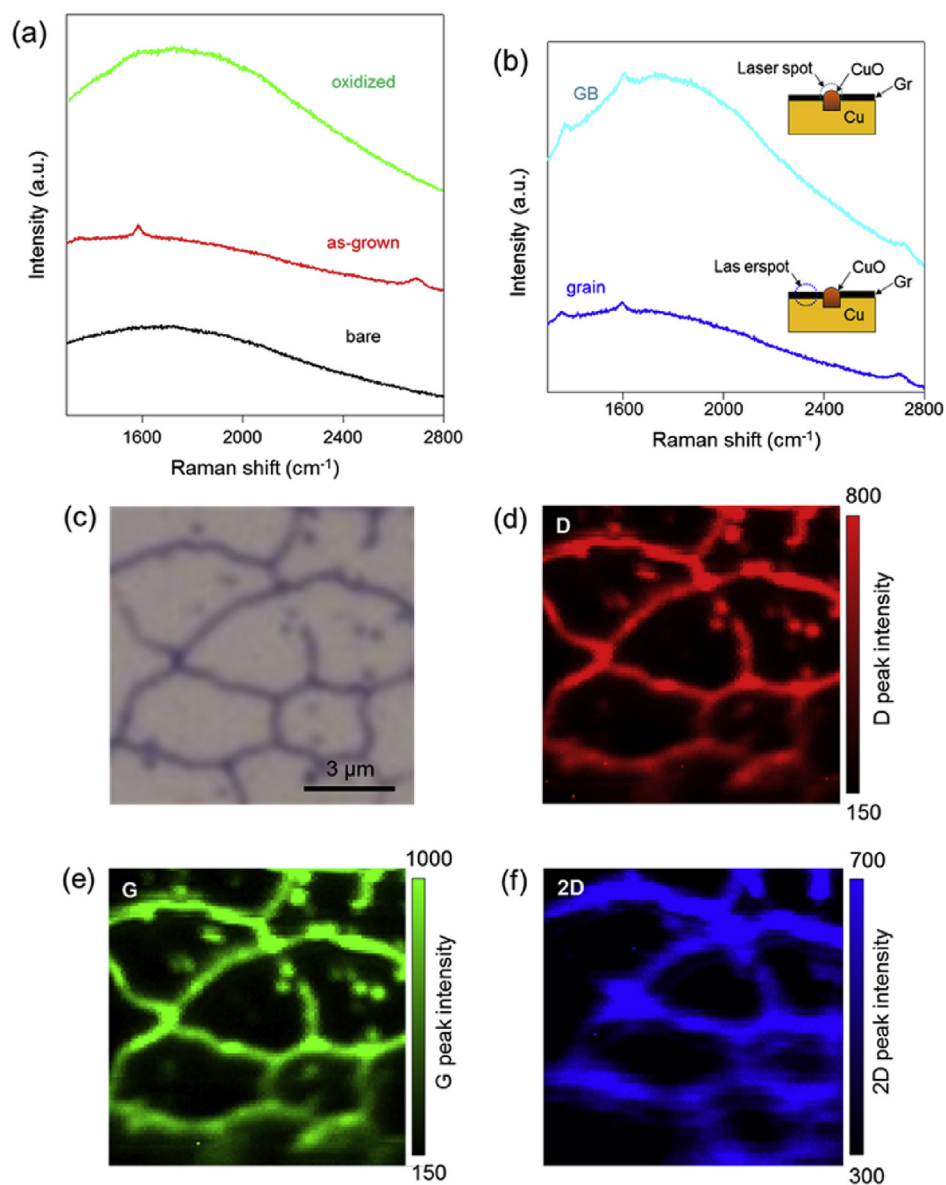


Fig. 3. (a) Raman spectra of bare copper before graphene growth (bare), graphene-grown copper (as-grown), and oxidized copper without graphene growth (oxidized). (b) Raman spectra of two regions of grain and GB in graphene-grown copper after PATO process. The inset schematics show two regions for Raman measurement. (c) Optical micrograph and Raman mapping images for (d) D, (e) G, and (f) 2D peaks.

parameters are mainly responsible for kinetic energy and behavior of plasma species [27,28]. More detailed sample preparation process is described in the experimental section. To further investigate the defect generation in various plasma treatment conditions, we measured Raman spectra of the transferred CVD graphene on SiO₂ substrate after plasma treatments. The Raman spectra of plasma-treated graphene are shown in Fig. 2. The as-grown graphene shows a prominent 2D peak at 2680 cm⁻¹, and no D peak near 1350 cm⁻¹, confirming its high quality. After plasma treatment of 10 s with varying plasma power (Fig. 2a), the D peak, which indicates the formation of defects, increased with the power. At the same time, 2D peak at 2680 cm⁻¹ becomes weaker and broader, indicating the loss of crystallinity in graphene. When the plasma treatment time was changed from 5 to 25 s with a fixed power of 50 W (Fig. 2b), defect density also increased with plasma time. To analyze the types of defects, we plotted peak intensity ratio of D and G peaks as shown in Fig. 2c and d. The D/G ratio has been used to examine the quality of graphene and the types of defects, such as sp³-type and vacancy-type defects [29,30]. Our Raman measurements show that the plasma treatment at low power or for short time mostly induces sp³-type defects. Beyond maximum D/G ratio, vacancy-type defects are generated as previously reported [29]. These are seen to emerge above 80 W plasma power and 15 s treatment time. Therefore, to selectively damage GBs and avoid creation of vacancy-type defects within grains, we selected an optimized plasma condition of 50 W and 10 s, which induces a moderate D/G ratio of 1.5–2. After the plasma treatment, the samples were heated on hot plate for oxidation of copper through the etched GBs. The oxidation process was optimized by varying the heating temperature (100–400 °C) and time (5–25 s) (Fig. S3). Fig. 2e shows typical optical micrographs of the oxidized samples following various heating conditions. As shown in the center image of the sample heated at 300 °C for 10 s, the locations of GBs can be obviously observed with orange lines. However, it is difficult to see the GBs in the samples heated in the other conditions due to the insufficient oxidation of copper at GBs or uniform oxidation of the entire copper. The optical images of oxidized copper can be digitalized for quantitative analysis, which enables us to quantitatively identify the GBs (Fig. S4).

Raman mapping was used to verify the location of GBs in the as-grown graphene films, as shown in Fig. 3. For comparison, we also prepared a copper foil before graphene growth (bare), graphene-grown copper (as-grown), and copper without graphene growth subjected to the same plasma treatment and heating used for GB visualization (oxidized) (Fig. 3a). All of bare copper, as-grown copper, and oxidized copper showed strong and broad background peaks over all the range of Raman spectra due to reflectance of metallic surface. Typically, background peak of the oxidized copper is stronger than that of the bare copper, which might be due to interferential enhancement of reflectance by thin copper oxide layer. After graphene growth, characteristic peaks of graphene (D, G and 2D) [31] appeared with a similar background signal of bare copper. After subsequent oxidation of copper through the GBs, the Raman spectra were measured from two regions of grain and grain boundary as depicted in the inset schematics of Fig. 3b. Even though background signals in both cases became stronger, the narrow copper area at GBs showed higher intensity due to accelerated oxidation of copper through the damaged GBs. The D peak was also enhanced in both areas due to additional generation of defects. After PATO process, these distinguishable differences in Raman spectra of the grain and GB regions enable us to produce Raman maps for microscale identification of GBs (Fig. 3d–f). In Raman mapping images, the intensities of D, G, and 2D peaks are strongly highlighted at GBs due to strong background signal of copper oxide under GB regions. When the background signal of

copper oxide was subtracted from the Raman spectra, we observed redshift and increase of Raman peaks after PATO as previously reported by Duong et al. [22] (Fig. S5). Nevertheless, It should be noted that our Raman mapping can be realized due to strong background signal from oxidized copper at GBs. After PATO process of as-grown graphene on copper, we transferred the treated graphene onto SiO₂ substrate. However, Raman maps showed no discernable GB region due to absence of strong background signal of copper oxide (Fig. S6). When as-grown graphene was transferred onto SiO₂ and then followed by the same PATO process, the GBs were not observed before and after PATO process (Figs. S7 and S8). When the Raman measurement was conducted on the CVD graphene area

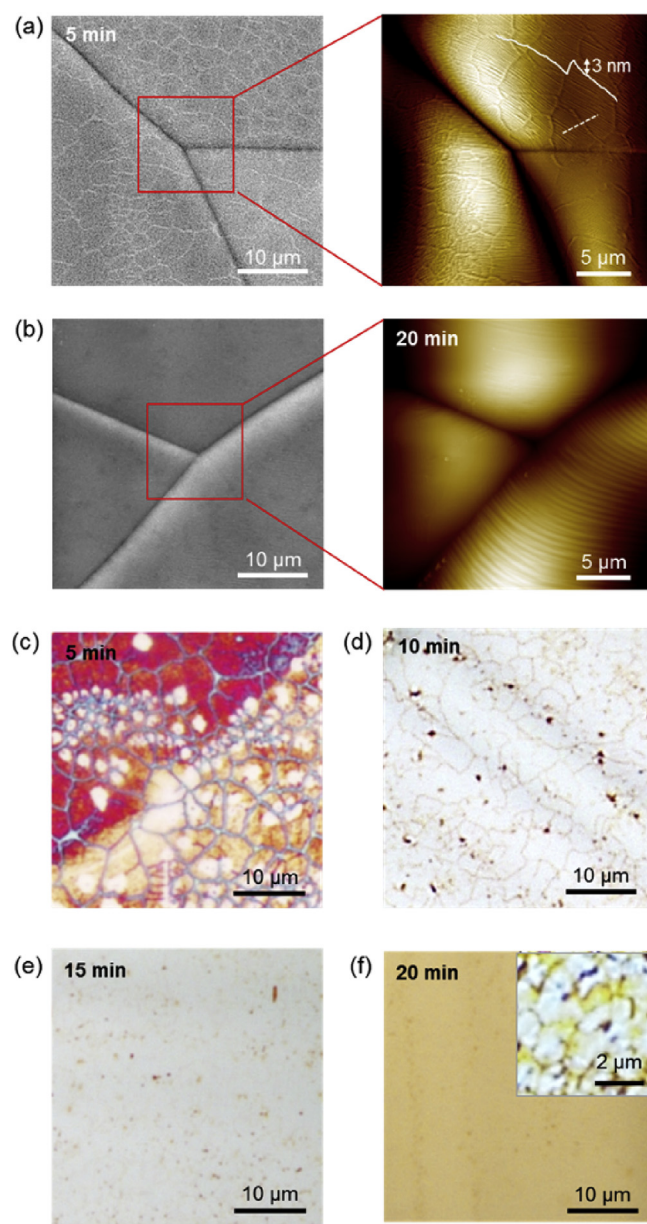


Fig. 4. SEM images of CVD graphene grown on a copper foil for (a) 5 min and (b) 20 min. The magnified AFM images of areas indicated by red lines are obtained for (a) and (b). The height profile of (a) measured along the dashed line shows naturally oxidized copper. Optical micrographs of the CVD graphene on copper foil grown for (c) 5, (d) 10, (e) 15, and (f) 20 min after PATO process. The inset of (f) shows optical micrograph of the 20 min-growth sample oxidized in harsher condition.

containing bilayer patches, the Raman mapping images showed significant difference between monolayer and bilayer regions, because copper under bilayer patch was less oxidized than monolayer region (Fig. S9). These results indicate that oxidation of copper through GBs is a key factor in our GB observation technique.

Fig. 4a and b shows surface morphologies of two CVD graphene samples grown for 5 and 20 min, measured by atomic force microscope (AFM) and scanning electron microscope (SEM). Although there is hardly any contrast under an optical microscope, clear lines are visible in the AFM and SEM images of 5-min growth sample, even without PATO process. These well-defined lines are in fact narrow gaps uncovered with graphene in between graphene grains of a few micrometers, where 3-nm thick oxide layer is naturally formed as shown in the AFM profile of Fig. 4a. On the contrary, the GBs were not seen in the 20-min growth sample before PATO process (Fig. 4b), as the GBs are well stitched without any gaps. Therefore, our GB observation technique can be utilized for evaluation of the quality of CVD graphene. For quality evaluation of CVD graphene, we prepared four CVD graphene samples grown for different time from 5 to 20 min as shown in Fig. 4c–f. The shorter growth time results in the smaller grain size and discontinuous boundaries (or nanogap) between grains, which degrade electrical conductivity and mechanical strength of CVD graphene, while the CVD graphene grown for a longer time has the larger grains and well-stitched GBs. Although no difference could be observed by optical microscope in the as-grown samples regardless of growth time, the GBs in the samples grown with shorter growth time became noticeable after PATO process with weaker conditions of oxygen plasma treatment (power = 50 W, time = 10 s) as graphene grains are not stitched, but there are small gaps between grains. On the contrary, when the same PATO process is performed to the graphene grown for a longer time, it showed no oxidation at GBs or any color change, indicating that the graphene grains are well-

stitched together. However, when harsher conditions of oxygen plasma treatment (power = 70 W, time = 10 s) and thermal oxidation was applied to high quality CVD graphene, GBs were able to be identified as shown in inset of Fig. 4f. Even though selective oxidation was utilized for visualization of GBs in the previous work by Duong et al. [22], our technique is more straightforward and fast. All PATO process can be finished within a minute without requirement of complicated process. Furthermore, our technique is useful for quality inspection of CVD-grown graphene, e.g. discontinuity at GBs, and identification of number of layers.

To better understand the atomic processes in graphene GBs and verify the preferential attack of oxygen plasma to GBs, we calculated the relative thermodynamic stabilities of various structures in graphene by using a first-principles density-functional theory (DFT) [24–26]. We first considered planar pristine graphene (Fig. 5a) and two large-angle GB structures along the armchair (Fig. 5b; with a grain angle of 32.2°) and zigzag (Fig. 5c; with a grain angle of 21.8°) directions – namely, a -32.2 and z -21.8, respectively [32]. Next, to mimic the possible local surface roughness, we introduced a small one-dimensional ridge to the planar structures along the armchair and zigzag directions as described by the sheet curvature index, κ (Supporting Information, Fig. S10). To assess the relative thermodynamic stability, we calculated the relative formation energy, ΔE as a function of κ (per unit length, with respect to pristine graphene) as shown in Fig. 5d. With the same value of curvature, GBs are energetically less stable than their defect-free counterparts, indicating that GBs are more prone to oxygen plasma attack than pristine graphene. Moreover, GBs become more unstable with increasing κ than pristine graphene. However, it is worth noting that pristine graphene with high local roughness (higher curvature) is more likely to be attacked by oxygen plasma than flat planar surface, as similarly reported in folds and bubbles [33–35]. Nevertheless, local oxidation of copper through

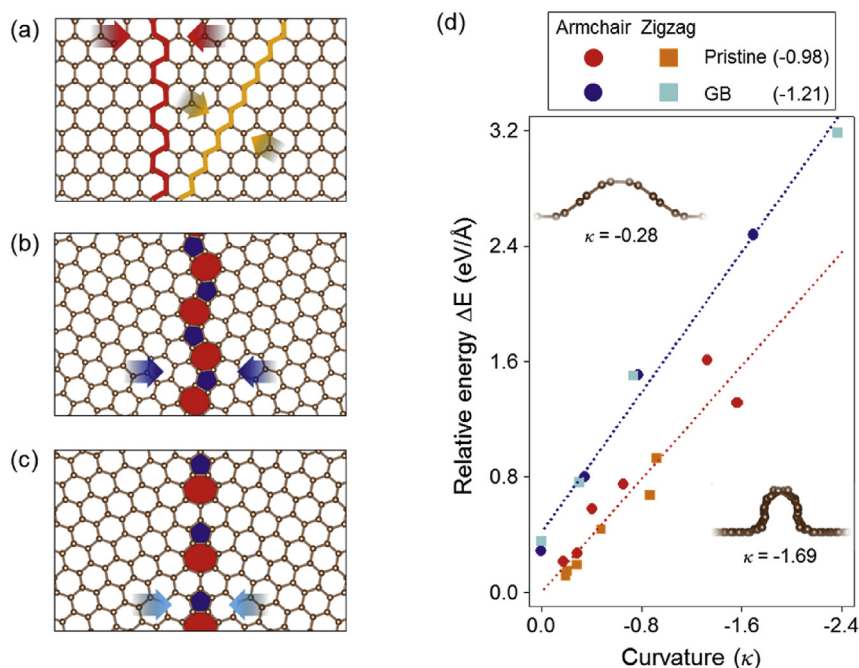


Fig. 5. (a–c) Top-view models of the atomic structures for pristine graphene (highlighting the armchair and zigzag directions) and the two direction-dependent GBs in graphene (highlighting the defect features). (d) The relative energy, ΔE (calculated with respect to the pristine graphene) is plotted as a function of sheet curvature (κ) for each graphene-based system. Folded graphene sheets are shown in the insets. For defect-free graphene, ΔE for one-dimensional folding in the armchair and the zigzag directions are shown in red and orange points, respectively. The blue and pale-blue points then represent the ΔE values for the two commonly observed grain boundaries (GBs) in graphene in the armchair and the zigzag directions, accordingly. Best-fit lines are shown for both pristine graphene (gradient of -0.98) and GBs (gradient of -1.21).

roughened pristine graphene, *i.e.* ripples, was not observed in our work due to absence of highly unstable ripples with a high curvature.

4. Conclusion

In summary, we report a novel yet straightforward technique for the direct observation of GBs in CVD graphene, which does not require complicated processes or expensive equipment. By selectively damaging graphene GBs using oxygen plasma and thermally oxidizing underlying copper through the defective GBs, the GBs can be clearly observed using a conventional optical microscope. The proposed GB observation technique does not only provide an economical mean to study microstructural characteristics of CVD graphene such as grain size, grain shape, and GBs, but also presents a method for highly efficient quality analysis of CVD graphene, making the large-scale graphene technology be more commercially viable.

Acknowledgements

This work was supported by Business for Cooperative R&D between Industry, Academy, and Research Institute funded Korea Small and Medium Business Administration in 2015 (C0351166), the Basic Science Research Program through the National Research Foundation of Korea funded by the Ministry of Science, ICT and Future Planning (2014R1A1A1004632), the third Stage of Brain Korea 21 Plus Project (Division of Creative Materials) in 2016 and Korea Research Fellowship Program through the National Research Foundation of Korea funded by the Ministry of Science, ICT and Future Planning(2016H1D3A1938061). J.-H. Lee and A. Soon was supported by the National Research Foundation of Korea through the government of Korea (MSIP) (NRF-2016R1A4A1012929). C.-H. Lee acknowledges the support from the Basic Science Research Program (NRF-2014R1A1A2055112) through the National Research Foundation (NRF) funded by the Korean Government Ministry of Education and KU-KIST Graduate School of Converging Science and Technology Program.

Appendix A. Supplementary data

Supplementary data related to this article can be found at <http://dx.doi.org/10.1016/j.carbon.2017.01.009>.

References

- [1] A.K. Geim, K.S. Novoselov, The rise of graphene, *Nat. Mater.* 6 (3) (2007) 183–191.
- [2] K.I. Bolotin, K.J. Sikes, Z. Jiang, M. Klima, G. Fudenberg, J. Hone, et al., Ultrahigh electron mobility in suspended graphene, *Solid State Commun.* 146 (9–10) (2008) 351–355.
- [3] G.H. Lee, R.C. Cooper, S.J. An, S. Lee, A. van der Zande, N. Petrone, et al., High-strength chemical-vapor-deposited graphene and grain boundaries, *Science* 340 (6136) (2013) 1073–1076.
- [4] R.R. Nair, P. Blake, A.N. Grigorenko, K.S. Novoselov, T.J. Booth, T. Stauber, et al., Fine structure constant defines visual transparency of graphene, *Science* 320 (5881) (2008) 1308.
- [5] N. Petrone, C.R. Dean, I. Meric, A.M. van der Zande, P.Y. Huang, L. Wang, et al., Chemical vapor deposition-derived graphene with electrical performance of exfoliated graphene, *Nano Lett.* 12 (6) (2012) 2751–2756.
- [6] S. Bae, H. Kim, Y. Lee, X. Xu, J.-S. Park, Y. Zheng, et al., Roll-to-roll production of 30-inch graphene films for transparent electrodes, *Nat. Nano* 5 (8) (2010) 574–578.
- [7] X. Li, C.W. Magnuson, A. Venugopal, R.M. Tromp, J.B. Hannon, E.M. Vogel, et al., Large-area graphene single crystals grown by low-pressure chemical vapor deposition of methane on copper, *J. Am. Chem. Soc.* 133 (9) (2011) 2816–2819.
- [8] X. Li, C.W. Magnuson, A. Venugopal, J. An, J.W. Suk, B. Han, et al., Graphene films with large domain size by a two-step chemical vapor deposition process, *Nano Lett.* 10 (11) (2010) 4328–4334.
- [9] Y. Hao, M.S. Bharathi, L. Wang, Y. Liu, H. Chen, S. Nie, et al., The role of surface oxygen in the growth of large single-crystal graphene on copper, *Science* 342 (6159) (2013) 720–723.
- [10] X. Li, W. Cai, J. An, S. Kim, J. Nah, D. Yang, et al., Large-area synthesis of high-quality and uniform graphene films on copper foils, *Science* 324 (5932) (2009) 1312–1314.
- [11] J.H. Lee, E.K. Lee, W.J. Joo, Y. Jang, B.S. Kim, J.Y. Lim, et al., Wafer-scale growth of single-crystal monolayer graphene on reusable hydrogen-terminated germanium, *Science* 344 (6181) (2014) 286–289.
- [12] F. Banhart, J. Kotakoski, A.V. Krasheninnikov, Structural defects in graphene, *ACS Nano* 5 (1) (2011) 26–41.
- [13] A.W. Tsen, L. Brown, M.P. Levendorf, F. Ghahari, P.Y. Huang, R.W. Havener, et al., Tailoring electrical transport across grain boundaries in polycrystalline graphene, *Science* 336 (6085) (2012) 1143–1146.
- [14] Q. Yu, L.A. Jauregui, W. Wu, R. Colby, J. Tian, Z. Su, et al., Control and characterization of individual grains and grain boundaries in graphene grown by chemical vapour deposition, *Nat. Mater.* 10 (6) (2011) 443–449.
- [15] O.V. Yazyev, S.G. Louie, Electronic transport in polycrystalline graphene, *Nat. Mater.* 9 (10) (2010) 806–809.
- [16] J. Lee, J. Baek, G.H. Ryu, M.J. Lee, S. Oh, S.K. Hong, et al., High-angle tilt boundary graphene domain recrystallized from mobile hot-wire-assisted chemical vapor deposition system, *Nano Lett.* 14 (8) (2014) 4352–4359.
- [17] X. Wu, G. Zhong, L. D'Arsie, H. Sugime, S. Esconjauregui, A.W. Robertson, et al., Growth of continuous monolayer graphene with millimeter-sized domains using industrially safe conditions, *Sci. Rep.* 6 (2016) 21152.
- [18] P.Y. Huang, C.S. Ruiz-Vargas, A.M. van der Zande, W.S. Whitney, M.P. Levendorf, J.W. Kevek, et al., Grains and grain boundaries in single-layer graphene atomic patchwork quilts, *Nature* 469 (7330) (2011) 389–392.
- [19] K. Kim, Z. Lee, W. Regan, C. Kisielowski, M.F. Crommie, A. Zettl, Grain boundary mapping in polycrystalline graphene, *ACS Nano* 5 (3) (2011) 2142–2146.
- [20] J.H. Son, S.J. Baek, M.H. Park, J.B. Lee, C.W. Yang, J.K. Song, et al., Detection of graphene domains and defects using liquid crystals, *Nat. Commun.* 5 (2014) 3484.
- [21] X.H. Kong, H.X. Ji, R.D. Piner, H.F. Li, C.W. Magnuson, C. Tan, et al., Non-destructive and rapid evaluation of chemical vapor deposition graphene by dark field optical microscopy, *Appl. Phys. Lett.* 103 (4) (2013) 043119.
- [22] D.L. Duong, G.H. Han, S.M. Lee, F. Gunes, E.S. Kim, S.T. Kim, et al., Probing graphene grain boundaries with optical microscopy, *Nature* 490 (7419) (2012) 235–239.
- [23] J.S. Choi, J.-S. Kim, I.-S. Byun, D.H. Lee, M.J. Lee, B.H. Park, et al., Friction anisotropy-driven domain imaging on exfoliated monolayer graphene, *Science* 333 (6042) (2011) 607–610.
- [24] Kresse G. *Comput. Matter Sci.* 6 (1996) 15; (d) G. Kresse, *Furthmuller, Phys. Rev. B* 54 (1996) 11,169.
- [25] G. Kresse, J. Furthmüller, Efficiency of ab-initio total energy calculations for metals and semiconductors using a plane-wave basis set, *Comput. Mater. Sci.* 6 (1) (1996) 15–50.
- [26] K. Jirř, R.B. David, M. Angelos, Chemical accuracy for the van der Waals density functional, *J. Phys. Condens. Matter* 22 (2) (2010) 022201.
- [27] T. Kavka, J. Gregor, O. Chumak, M. Hrabovsky, Effect of arc power and gas flow rate on properties of plasma jet under reduced pressures, *Czechoslov. J. Phys.* 54 (3) (2004) C753–C758.
- [28] S.H. Lee, F. Iza, J.K. Lee, Particle-in-cell Monte Carlo and fluid simulations of argon-oxygen plasma: comparisons with experiments and validations, *Phys. Plasmas* 13 (5) (2006) 057102.
- [29] A. Zandiatashbar, G.H. Lee, S.J. An, S. Lee, N. Mathew, M. Terrones, et al., Effect of defects on the intrinsic strength and stiffness of graphene, *Nat. Commun.* 5 (2014) 3186.
- [30] A. Eckmann, A. Felten, A. Mishchenko, L. Britnell, R. Krupke, K.S. Novoselov, et al., Probing the nature of defects in graphene by Raman spectroscopy, *Nano Lett.* 12 (8) (2012) 3925–3930.
- [31] A.C. Ferrari, D.M. Basko, Raman spectroscopy as a versatile tool for studying the properties of graphene, *Nat. Nanotechnol.* 8 (4) (2013) 235–246.
- [32] O.V. Yazyev, S.G. Louie, Topological defects in graphene: dislocations and grain boundaries, *Phys. Rev. B* 81 (19) (2010) 195420.
- [33] W. Zhu, T. Low, V. Perebeinos, A.A. Bol, Y. Zhu, H. Yan, et al., Structure and electronic transport in graphene wrinkles, *Nano Lett.* 12 (7) (2012) 3431–3436.
- [34] J. Zabel, R.R. Nair, A. Ott, T. Georgiou, A.K. Geim, K.S. Novoselov, et al., Raman spectroscopy of graphene and bilayer under biaxial strain: bubbles and balloons, *Nano Lett.* 12 (2) (2012) 617–621.
- [35] T. Georgiou, L. Britnell, P. Blake, R.V. Gorbachev, A. Gholinia, A.K. Geim, et al., Graphene bubbles with controllable curvature, *Appl. Phys. Lett.* 99 (9) (2011) 093103.

Supporting Information

Direct Observation of Grain Boundaries in Chemical Vapor Deposited Graphene

Jong-Young Lee^a, Ji-Hwan Lee^a, Min Jung Kim^a, Jatis Kumar Dash^a, Chul-Ho Lee^b, Rakesh Joshi^c, Sunwoo Lee^d, James Hone^e, Aloysius Soon^a, and Gwan-Hyoung Lee^{a,}*

^a Department of Materials Science and Engineering, Yonsei University, Seoul 03722, Korea

^b KU-KIST Graduate School of Converging Science and Technology, Korea University, Seoul 02841, Korea

^c Centre for Sustainable Materials Research and Technology (SMART), School of Materials Science and Engineering, University of New South Wales, Sydney 2052, Australia

^d Department of Electrical and Computer Engineering, Cornell University, Ithaca, NY 14853, USA

^e Department of Mechanical Engineering, Columbia University, New York, NY 10027, USA

* E-mail address: gwanlee@yonsei.ac.kr (Gwan-Hyoung Lee)

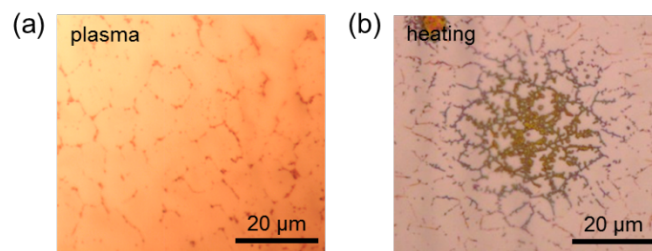


Fig. S1. Optical micrographs of graphene-grown copper foils oxidized with different methods. (a) Oxygen plasma treatment and (b) thermal oxidation (heating). When graphene-grown copper foil was treated by oxygen plasma for a short time, copper was not fully oxidized, while, when it was treated for a long time, graphene was etched away so quickly. When the as-grown sample was heated at 300 °C without pre-treatment of oxygen plasma, local oxidation of copper was seen. Therefore, it is difficult to clearly observe GBs by just exposing the sample under oxygen plasma or heating the sample.

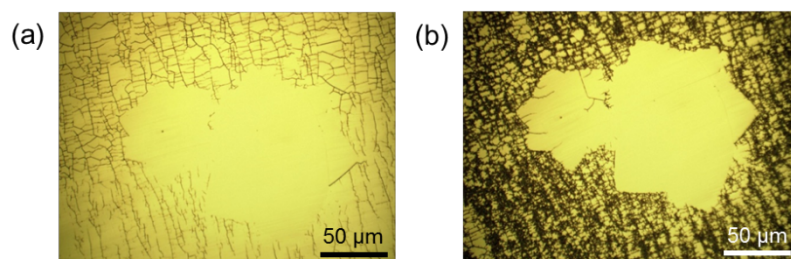


Fig. S2. Optical micrographs of graphene-grown copper foils consisting of large grains of multilayers. The sample was oxidized by just heating it at 300 °C for (a) 1 min and (b) 5 min.


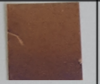
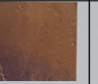

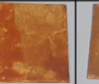
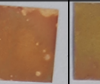

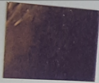
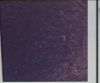



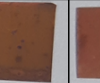
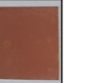

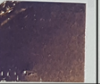

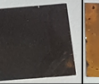
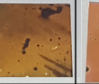
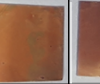


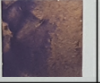

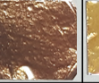

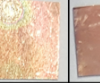




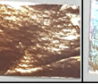



| Temp. (°C) \ time (s) | 100 | 150 | 20 | 250 | 300 | 350 | 400 |
|-----------------------|---|---|---|---|--|---|---|
| 5 |  |  |  |  |  |  |  |
| 10 |  |  |  |  |  |  |  |
| 15 |  |  |  |  |  |  |  |
| 20 |  |  |  |  |  |  |  |
| 25 |  |  |  |  |  |  |  |

Fig. S3. Optical images of graphene-grown copper foils after PATO process with different temperatures and times.

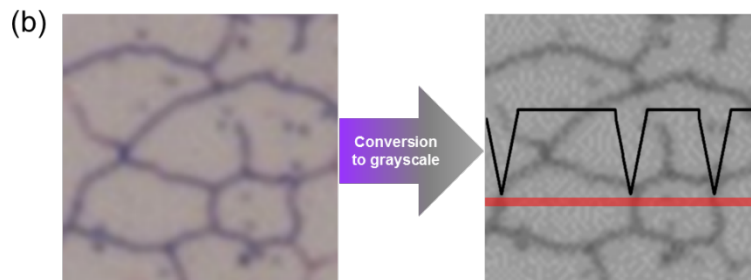
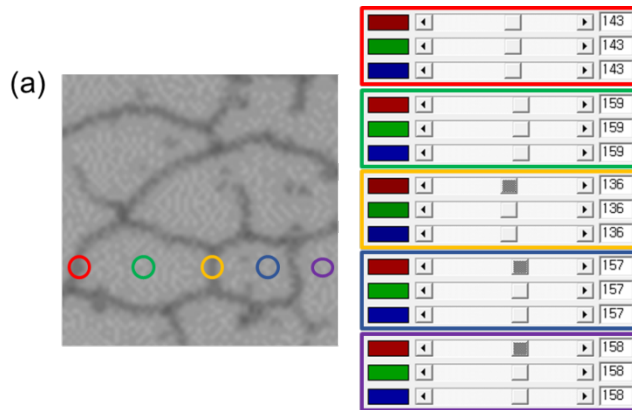


Fig. S4. Quantitative analysis of the optical image. (a) RGB values from each pixel (circles) and calculation of grayscale value by $\text{grayscale} = (R+G+B)/3$. (b) Conversion of the optical image to monochrome image. The line profile of grayscale value shows positions of grain boundaries.

To compare Raman spectrum of graphene without copper oxide, the background signal was removed from the Raman spectra (Fig. 3), the D peak of GB region is higher compared to as-grown graphene and grain region (Fig. S4), indicating that defective GBs of graphene are more susceptible to the external reaction (*i.e.* oxygen plasma) compared to grains of perfect honeycomb structure. Both G and 2D peaks were red shifted after oxidation. Larger shift of GB region can be explained in terms of tensile strain applied to graphene by formation of copper oxide layer with larger volume and doping by oxygen species attached to GBs [1-4].

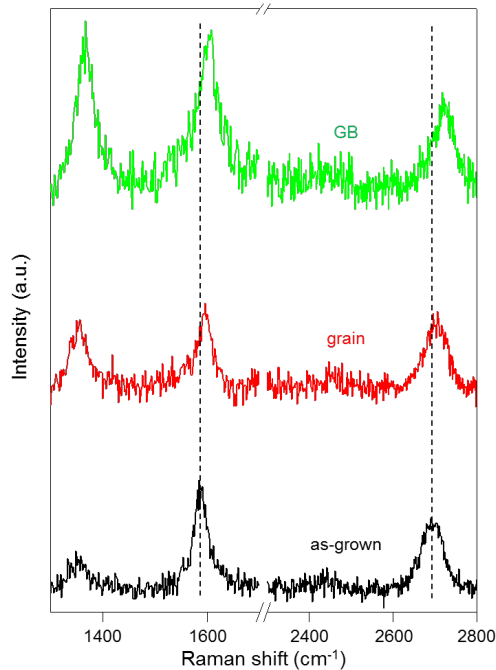


Fig. S5. Raman spectra of as-grown CVD graphene (as-grown), grain, and GB after PATO process. The subtract background signal was subtracted from the Raman spectra.

To prove the contribution of copper substrate to GB observation, we prepared three different graphene samples and performed Raman measurements with PATO process for each sample. Fig. S5 shows (a) optical micrograph, (b-d) Raman mapping images, and (e) Raman spectrum of CVD graphene transferred on SiO₂ substrate after PATO process. As shown in Fig. 3, GB region on Cu substrate has enhanced Raman intensity after PATO process. However, after transferred on SiO₂ substrate, GBs were not observed through optical microscope and Raman mapping images. These results indicate that GB observation through PATO process is highly related to the oxidation of copper at GBs. As expected, when CVD graphene was transferred and treated by

PATO process, CVD graphene showed typical Raman mapping images and spectrum as shown in Fig. S6 and S7. However, there was no significant difference in optical micrograph and GBs were not observed through Raman mapping images. Although GB of CVD graphene is thermodynamically unstable to react with oxygen, the defective carbon through specific reaction between GB and oxygen is too small to observe using microscopic measurement system. From these results, we confirmed copper substrate is necessary to observe GB through PATO process.

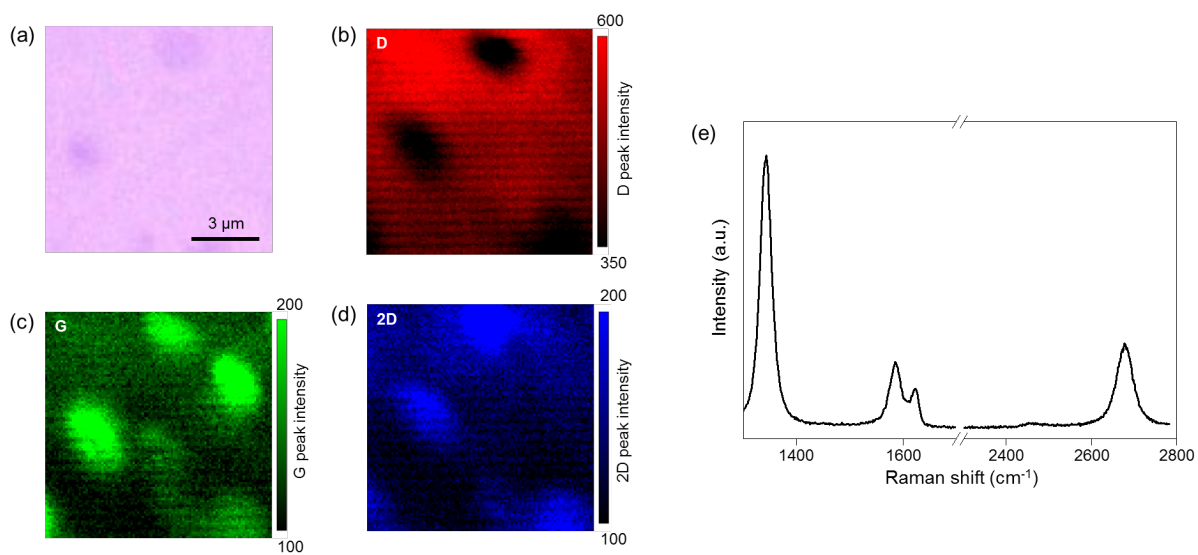


Fig. S6. (a) Optical micrograph, Raman mapping images for (b) D, (c) G, and (d) 2D peaks, and (e) Raman spectrum of CVD graphene transferred onto SiO₂ substrate after PATO process.

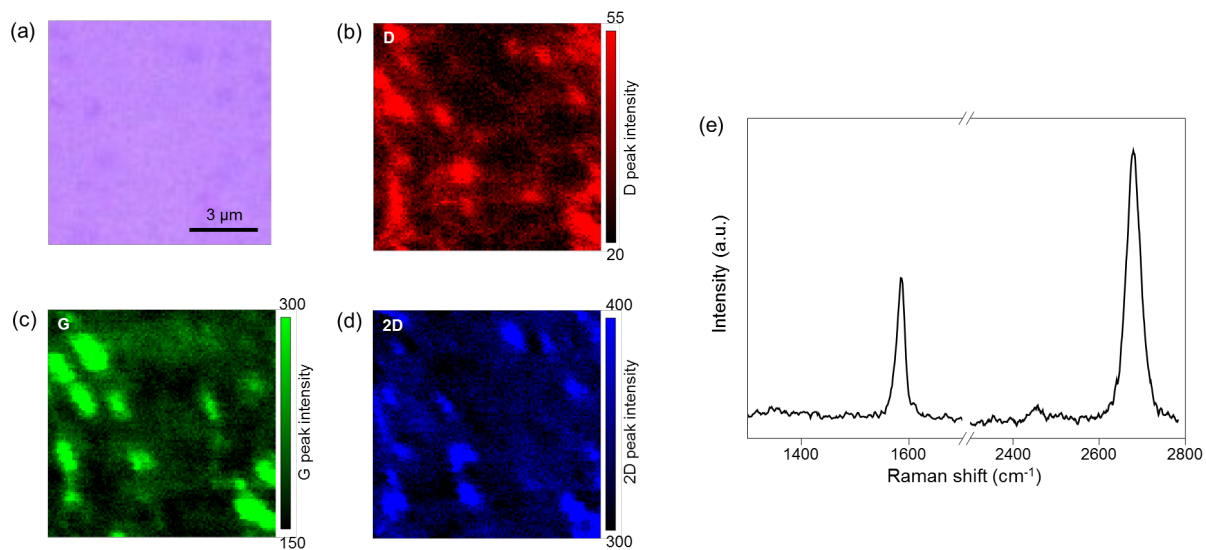


Fig. S7. (a) Optical micrograph, Raman mapping images for (b) D, (c) G, and (d) 2D peaks, and (e) Raman spectrum of CVD graphene transferred onto SiO₂ substrate without any treatment.

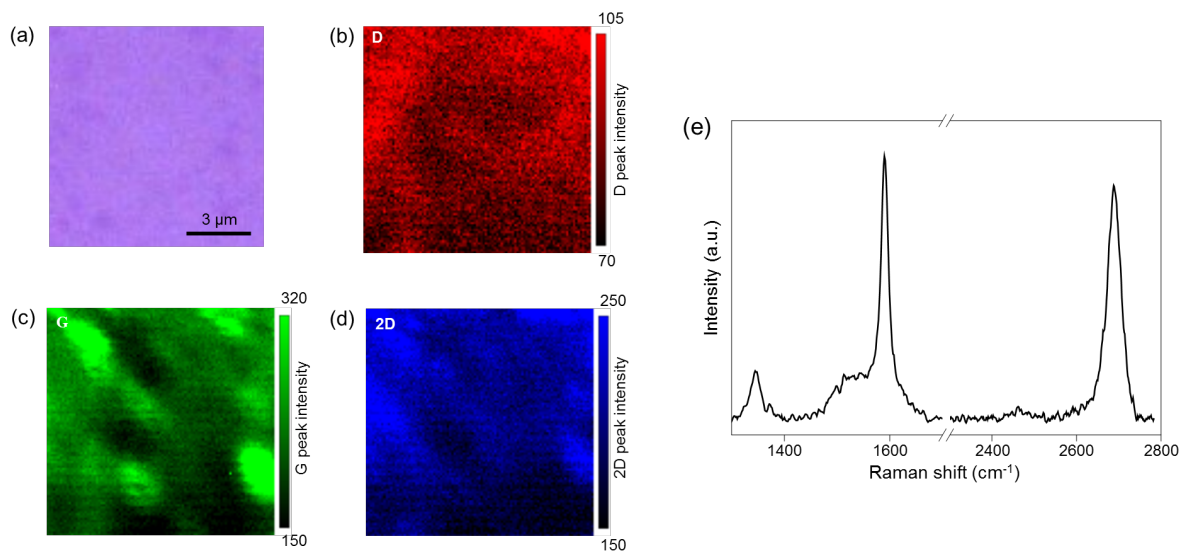


Fig. S8. (a) Optical micrograph, Raman mapping images for (b) D, (c) G, and (d) 2D peaks, and (e) Raman spectrum of CVD graphene transferred onto SiO₂ substrate, then treated by PATO process.

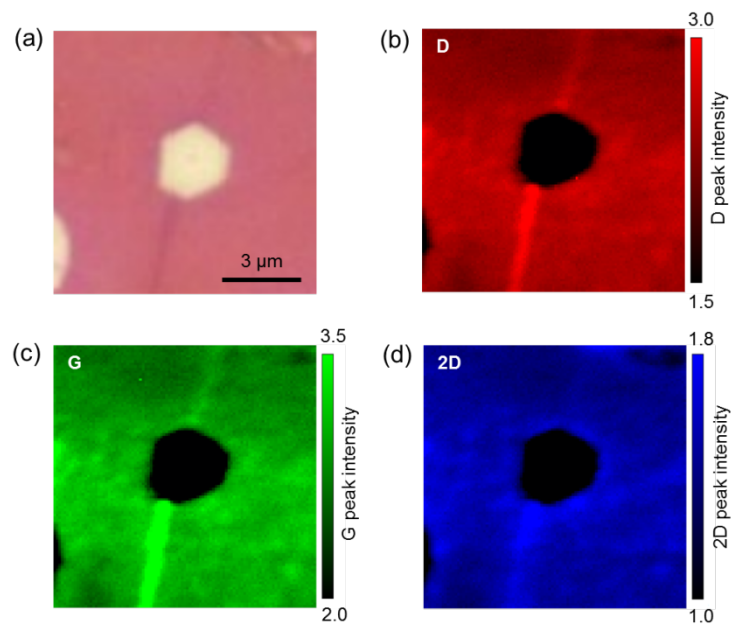


Fig. S9. (a) Optical micrograph and Raman mapping images for (b) D, (c) G, and (d) 2D peaks of CVD graphene with bilayer patches after PATO process. Brighter optical image and quenched Raman intensity of bilayer region indicates different oxidation rate for monolayer and bilayer.

For DFT calculations, a Γ -centered \mathbf{k} -point grid of $19 \times 19 \times 1$ is used for the $p(1 \times 1)$ unit cell of pristine graphene, and the \mathbf{k} -point grid is then folded accordingly for the larger supercells used in our calculations. To minimize spurious interactions between neighboring cells in the z -direction, a vacuum region of at least 18 \AA is enforced.

Using the optB88-vdW xc functional, the lattice constants for graphite are calculated to be 2.47 \AA for a axis and 6.68 \AA for c -axis. Likewise, the lattice constant and cohesive energy of bulk Cu are found to be 3.62 \AA and 3.56 eV/atom . Our results agree well with previous theoretical and experimental reports [5, 6].

To mimic the commensurate physisorbed graphene layer on Cu(111), we have applied a tensile strain ($\sim 3\%$) on the graphene layer to match the surface lattice constants of Cu(111). Here, we find that the adsorption energy of graphene on Cu(111) is indeed very weak (0.67 meV/C atom) and with a rather large vertical adsorption distance of 3.27 \AA . This is in good agreement with previous studies [7] and in this work, as a first step, we neglected the influence of the Cu(111) substrate in our calculations. To mimic the grain boundaries (GBs) found in our experiments, we refer to Yazyev et al. [8] and consider two large-angle GBs along the armchair (with a grain angle of 32.2°) and zigzag (with a grain angle of 21.8°) directions – namely, a - 32.2 and z - 21.8 , respectively. To model the local surface roughness observed in experiments, we have created a one-dimensional “*ridge*” to the planar structures (i.e. a *fold* as described by a sheet curvature index, κ ; see below) along both the armchair and zigzag while keeping the symmetry of system centered about the position of fold.

During geometry optimization, we fully relax the C atoms near the center of fold (i.e. ranging from 4 to 8 \AA from the center of the fold) while keeping all other C atoms fixed to their planar positions. This results in a lateral distance of more than 10 \AA between the folds to minimize their lateral interaction.

In order to compare the relative thermodynamic stability for each graphene-based system [9, 10], we calculate the relative energy (per unit length), ΔE as follows:

$$\Delta E = \frac{E_{\text{tot}} - NE^{\text{Pristine}}}{l}$$

where E_{tot} is total energy of graphene-based system, N is a total number of C atoms in the system, and E^{Pristine} is total energy (per C atom) of pristine graphene. The calculated ΔE for planar z -21.8 and a -32.2 are found to be 0.33 and 0.20 eV/Å, respectively.

As shown in Fig. 3, the sheet curvature index, κ is calculated by performing a simple differentiation to a 2nd order polynomial fit of the z -coordinates of the C atoms as projected in the direction perpendicular to the fold. The following quadratic equation is used:

$$h(x) = ax^2 + bx + c,$$

$$\kappa = \frac{d^2h}{dx^2} = 2a$$

where $h(x)$ is height of z -coordinates of the C atoms taken as a 2nd order polynomial function of x values along b -axis.

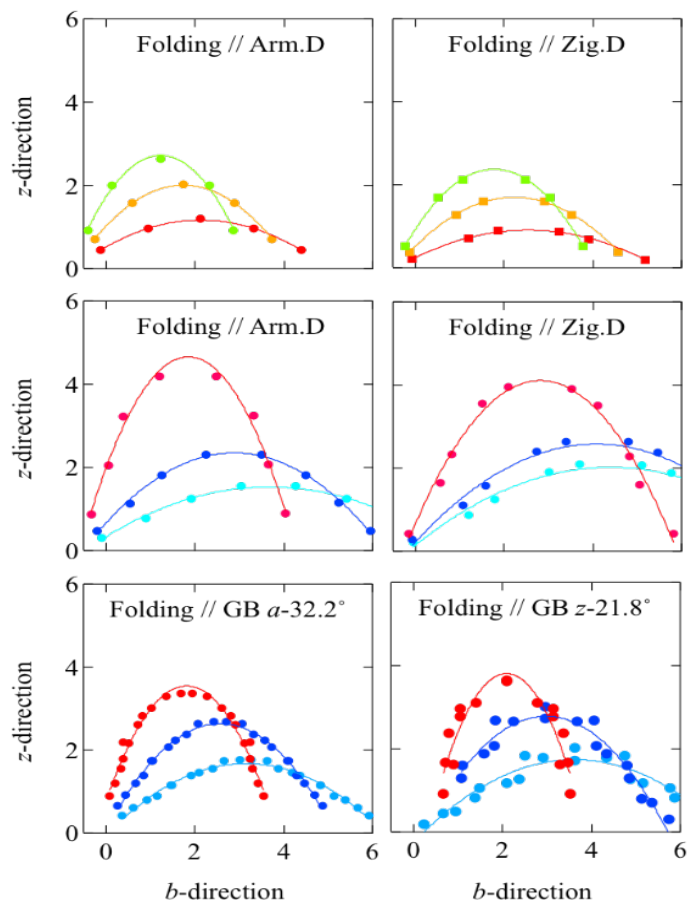


Fig. S10. Fitted plots of z-coordinates of C atoms near the center of the induced fold parallel to the armchair (Arm.D) and zigzag (Zig.D) directions for pristine graphene and GBs at different fold heights (and thus, sheet curvature index, κ). Values here are reported in Å. To derive the κ values for each case, a 2nd order polynomial fitting is performed for each case and the fitted curve is shown accordingly.

References

- [1] Malard LM, Pimenta MA, Dresselhaus G, Dresselhaus MS. Raman spectroscopy in graphene. *Physics Reports*. 2009;473(5–6):51-87.
- [2] Huang M, Yan H, Chen C, Song D, Heinz TF, Hone J. Phonon softening and crystallographic orientation of strained graphene studied by Raman spectroscopy. *Proceedings of the National Academy of Sciences*. 2009;106(18):7304-8.
- [3] Jin Z, McNicholas TP, Shih C-J, Wang QH, Paulus GLC, Hilmer AJ, et al. Click Chemistry on Solution-Dispersed Graphene and Monolayer CVD Graphene. *Chemistry of Materials*. 2011;23(14):3362-70.
- [4] Güneş F, Han GH, Shin H-J, Lee SY, Jin M, Duong DL, et al. UV-LIGHT-ASSISTED OXIDATIVE sp³ HYBRIDIZATION OF GRAPHENE. *Nano*. 2011;06(05):409-18.
- [5] Lee J-H, Park J-H, Soon A. Assessing the influence of van der Waals corrected exchange-correlation functionals on the anisotropic mechanical properties of coinage metals. *Physical Review B*. 2016;94(2):024108.
- [6] Björkman T. Testing several recent van der Waals density functionals for layered structures. *The Journal of Chemical Physics*. 2014;141(7):074708.
- [7] Ferrighi L, Trioni MI, Di Valentin C. Boron-Doped, Nitrogen-Doped, and Codoped Graphene on Cu(111): A DFT + vdW Study. *The Journal of Physical Chemistry C*. 2015;119(11):6056-64.
- [8] Yazyev OV, Louie SG. Topological defects in graphene: Dislocations and grain boundaries. *Physical Review B*. 2010;81(19):195420.
- [9] Jang W, Kang K, Soon A. Remarkably low-energy one-dimensional fault line defects in single-layered phosphorene. *Nanoscale*. 2015;7(45):19073-9.
- [10] Singh A, Waghmare UV. Structural instabilities and wrinkles at the grain boundaries in 2-D h-BN: a first-principles analysis. *Physical Chemistry Chemical Physics*. 2014;16(39):21664-72.